Applied Catalysis A, General 558 (2018) 91–98

Contents lists available at ScienceDirect

Applied Catalysis A, General

journal homepage: www.elsevier.com/locate/apcata

Multicomponent Au/Cu-ZnO-Al_2O_3 catalysts: Robust materials for clean hydrogen production

J.L. Santos[a], T.R. Reina[b,*], I. Ivanov[c], A. Penkova[a], S. Ivanova[a,*], T. Tabakova[c], M.A. Centeno[a], V. Idakiev[c], J.A. Odriozola[a]

[a] Departamento de Química Inorgánica, Universidad de Sevilla e Instituto de Ciencias de Materiales de Sevilla Centro mixto US-CSIC Avda., Américo Vespucio 49, 41092 Seville, Spain
[b] Department of Chemical Engineering and Process Engineering, University of Surrey, Guildford, GU2 7XH, United Kingdom
[c] Institute of Catalysis, Bulgarian Academy of Sciences, 5 Acad. G. Bonchev str., 1113 Sofia, Bulgaria

ARTICLE INFO

Keywords:
H_2 energy
Gold catalysts
Copper-Zinc catalysts
Hydrotalcite
WGS

ABSTRACT

Clean hydrogen production via WGS is a key step in the development of hydrogen fuel processors. Herein, we have designed a new family of highly effective catalysts for low-temperature WGS reaction based on gold modified copper-zinc mixed oxides. Their performance was controlled by catalysts' composition and the Au-Cu synergy. The utilization of hydrotalcite precursors leads to an optimal microstructure that ensures excellent Au and Cu dispersion and favors their strong interaction. From the application perspective these materials succeed to overcome the major drawback of the commercial WGS catalysts: resistance towards start/stop operations, a mandatory requisite for H_2-powered mobile devices.

1. Introduction

Although, one of the most studied throughout the history of catalytic reactions, the water gas shift (WGS) still present challenges, which makes necessary further research on its regard [1]. The renewed interest on this reaction is provoked by the search for new technologies for more efficient and greener energy carriers' production.

In this scenario, the WGS ($CO + H_2O \leftrightarrow CO_2 + H_2$) is the most successful combination of H_2 production and environmentally friendly CO gas depletion [2]. However, to take advantage on both processes the hydrogen should be produced from hydrocarbons, or biomass by reforming reactions where the H_2 and CO are produced [3]. Hydrogen enrichment of the streams are then envisaged through the WGS reaction meanwhile the CO concentration is reduced to a possible minimum [4,5]. As exothermic equilibrium reaction, the WGS involved different constraints that make necessary the operation at low-temperature at very low reaction rates. The success of the on board application of the post reforming WGS units is based on development of the catalyst working efficiently at low temperature conditions [6].

Typically, Cu/ZnO/Al_2O_3 catalysts are used for low temperature WGS reaction [7,8]. However, these catalysts present an important disadvantage - their pyrophoricity. The use of noble metals is also broadly studied as alternative to Cu based catalysts [6,9–11]. All Pt group based catalysts work at suitable temperature to be successfully considered but need special conditions of pre-treatment and show important deactivation, if water condensation occurs abruptly during shutdown [12,13]. On the contrary, gold-based catalysts can be used as prepared but at temperatures higher than the range shown by Pt [14]. Until now, none of the proposed alternatives seems to convince the scientific community to be selected as Cu-Zn-Al successor, especially considering WGS units designed for mobile on-board H_2 production. Recently, the combination of copper-zinc hydrotalcite (HT) material and gold was proposed as effective catalyst for the WGS [6]. However, these materials are deactivated when start/stop cycles are performed. Further catalyst' improvement should then proceed through active phase composition adjust. The latter in principle should optimize also catalyst' stability and H_2 yield either by lowering the temperature of operation or by increasing the activity/stability ratio at equilibrium conversion. A way to optimize the active phase is to vary either the method of gold deposition in order to obtain catalyst with lower particles size and higher contact perimeter or to change active composition (metal ratio).

In this sense, the aim of this paper is to optimize the Au/Cu-ZnO-Al_2O_3 system performance by varying the active components ratio and the gold catalyst preparation method. The correlation between Au/Cu ratio, catalyst structure, redox behaviour, catalytic activity and stability are also discussed.

* Corresponding authors.
E-mail addresses: t.ramirezreina@surrey.ac.uk (T.R. Reina), svetlana@icmse.csic.es (S. Ivanova).

https://doi.org/10.1016/j.apcata.2018.04.002
Received 14 November 2017; Received in revised form 1 March 2018; Accepted 3 April 2018
Available online 04 April 2018

2. Experimental section

2.1. Catalysts preparation

2.1.1. Cu/ZnO/Al_2O_3 mixtures

Catalysts based on Cu/ZnO/Al_2O_3 hydrotalcites were synthetized by a conventional co-precipitation process at low saturation as described in the literature [15,16]. Aqueous solutions of $Cu(NO_3)_2{\cdot}2H_2O$, $Zn(NO_3)_2{\cdot}6H_2O$, $Al(NO_3)_3{\cdot}9H_2O$ (Sigma Aldrich) in necessary proportions were used as precursors to obtain different M2+/M3+ (Cu^{2+} + Zn^{2+}/Al^{3+}) ratios. The hydrotalcite structures were formed with aqueous 1 M Na_2CO_3 (Sigma Aldrich) added dropwise to the precursor's mixture until pH rises to 8. Then pH was maintained during 48 h using an automatic burette (Crisol pH-Burette 24). After that time, the precipitated solid was separated by filtration, washed abundantly with distilled water and dried overnight at 90 °C. Thus, three hydrotalcite supports were prepared with constant (Cu/Zn) ratio of 5.6 and varying M^{2+}/M^{3+} ratio of 1, 2 and 3.

Prior use the hydrotalcite samples were calcined in static air at 300 °C during 2 h at 5 °C/min heating rate. For simplicity, the zinc was omitted from the labels and the obtained samples were labelled HTCu1; HTCu2; HTCu3.

2.1.2. Gold deposition

Gold catalysts were prepared by deposition-precipitation method in a "Contalab" (Contraves AG, Switzerland) reactor assuring full control of pH, temperature, stirring rate, and reactant feed flow [17]. Briefly, gold was deposited via chemical interaction between $HAuCl_4{\cdot}3H_2O$ precursor and Na_2CO_3, under vigorous stirring, maintaining constant pH of 7 and temperature 60 °C. After filtering and washing, the catalysts were dried under vacuum and calcined in air at 300 °C for 2 h. The nominal gold amount was 3 wt.% Au.

Similarly, the gold catalysts were labelled AuHTCu1, AuHTCu2 and AuHTCu3 corresponding to parent hydrotalcite structures.

2.2. Experimental techniques

X-ray microfluorescence spectrometry (XRMF) using EDAX Eagle III spectrophotometer with rhodium source of radiation was employed to determine the chemical compositions of the solids.

X-ray diffraction (XRD) analysis was carried out on X`Pert Pro PANalytical instrument using Cu Kα radiation (40 mA, 45 kV) and position-sensitive detector over a 2Θ-range from 10 to 90° using step size of 0.05° and corresponding step time of 240 s.

Particles size and distributions were measured by high resolution transmission electron microscopy (HR-TEM) performed on a FEI Talos electron microscope operated at an acceleration voltage of 200 kV, equipped with a Field Emission filament. Digital images were taken with a side mounted Ceta 16 M camera. For HR-TEM preparation a few milligrams of each sample were deposited directly on 300 mesh holey carbon coated copper free TEM-grid. The mean particles sizes were estimated from HR-TEM micrographs by single particle measurement of at least 200 particles. Mapping analysis was taken by S/TEM mode. The average gold particle size was estimated considering the surface distribution calculation, expressed in Eq. (1).

$$D[3,2] = \frac{\sum_1^n D_i^3 v^i}{\sum_1^n D_i^2 v^i} \quad (1)$$

where Di is the geometric diameter of the ith particle, and vi the number of particles with this diameter.

The Temperature Programmed Reduction (TPR) experiments were carried out in conventional quartz reactor coupled with thermal conductivity detector (TCD). The reactive gas stream, 5% H2 in Ar (Air Liquide) was passed through a 50 mg of sample loaded into the reactor with a flow rate of 50 ml min^{-1} and the temperature rose at 10 °C min^{-1} from room temperature to 900 °C. Molecular sieve 13X was used to retain the H_2O produced during the reduction.

XPS experiments were carried out on SPECS spectrometer equipped with PHOIBOS 150 MCD analyzer working with fixed pass energy of 40 eV and 1.0 eV of resolution. As monochromatic source of radiation Al Kα radiation (1486.6 eV) was used working on 250 W and 12.5 kV voltage. The analytical chamber operates at ultra-high vacuum at around 10^{-10} mbar pressure. The samples were introduced in XPS analysis chamber after different pretreatments. The pretreatments include pre-chamber conditioning at 10^{-8} mbar and activation in high-pressure treatment cell (HTHP Cell) under heating at 150 °C for 1 h. After cooling to room temperature, the first spectrum is taken and designed as RT. Then the samples were gradually reduced at three different temperatures (150,250 and 350 °C) during 1 h in 5%H_2/Ar mixture. After reduction, the evacuation of the gases was maintained overnight and before the spectrum acquisition, the samples were reheated to the corresponding temperature under vacuum. Since $Zn2p_{3/2}$ photoelectron peak is strong and its binding energy (BE) is virtually insensitive to its chemical states zinc (Zn $2p_{3/2}$ = 1021.1 eV) was used as internal standard.

2.3. Catalytic activity

Water gas shift reaction was performed in stainless steel tubular flow reactor (internal diameter of 0.7 cm) at atmospheric pressure in the 140–350 °C temperature range, using two reaction mixtures called "model" and "post-reforming" conditions. The "model" conditions (4.5%CO, 30% H_2O and N_2 as balance) are the ones usually employed for pure H_2 production whereas the "realistic" conditions (9% CO, 30% H_2O, 11% CO_2 and 50% H_2) can be designed as CO clean-up conditions after reforming step. The catalysts pelletized and sieved within the 600–800 μm range are employed for the test at constant catalyst bed volume in order to obtain gas hour space velocity of 2000 and 4000 h^{-1} (GHSV defined as total gas flow*catalyst volume*hour). CO and CO_2 contents were analysed on-line with an ABB gas analyzer and the activity is expressed in terms of CO conversion. No activation procedures were employed prior the reaction.

3. Results and discussion

Experimental procedure for catalysts preparation and their corresponding labels are described on the experimental section.

3.1. Chemical composition

The chemical composition of the samples expressed in % wt. is presented in Table 1.

M^{2+}/M^{3+} ratio gradually increases along the series from 1 to 3 as intended to obtain in the synthesis procedure. The samples also maintain the desired Cu/Zn ratio and the gold loadings are close to the targeted value of 3 wt.% and are very similar among the studied series.

Table 1
Chemical composition of the prepared mixed samples.

Sample	Au (% wt.)[a]	Cu^{2+}/Zn^{2+}[b]	$Cu^{2+}+Zn^{2+}/Al^{3+}$[b]
HTCu1	–	5.9 ± 0.05	1.2 ± 0.05
HTCu2	–	6 ± 0.05	1.9 ± 0.05
HTCu3	–	5.6 ± 0.05	2.8 ± 0.05
AuHTCu1	2.7 ± 0.07	6.1 ± 0.05	0.9 ± 0.05
AuHTCu2	2.8 ± 0.02	5.2 ± 0.05	2 ± 0.05
AuHTCu3	2.6 ± 0.04	5.4 ± 0.05	2.9 ± 0.05

[a] ICP.
[b] Fluorescence X Ray.

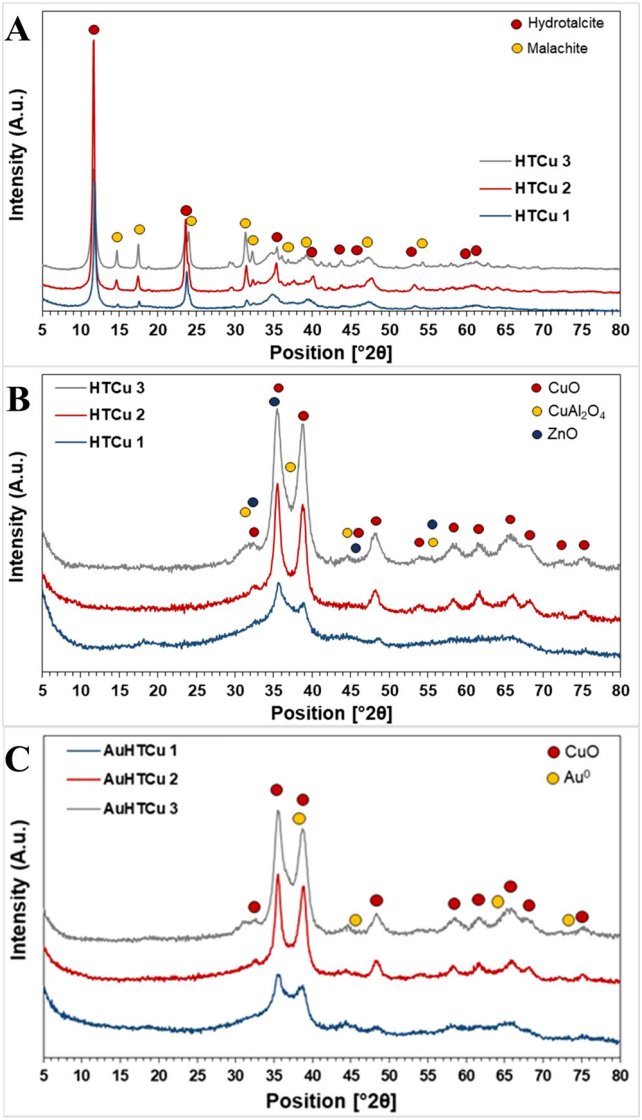

Fig. 1. A.)XRD patterns before calcination (fresh samples). **B.)** XRD patterns of the calcined supports. **C.)** XRD patterns gold based catalysts.

3.2. XRD

X-Ray diffraction was used to analyze the crystalline phase composition of the prepared materials. Fig. 1 shows the X-Ray diffraction patterns of the samples at different stages of their use, e.g. fresh and calcined and post gold deposition. XRD profiles of the fresh HTCu samples (Fig. 1A) revealed the presence of laminar hydrotalcite structure (JCPDS#37-0629) confirmed by the diffractions registered around 12 and 24° 2Θ.

These reflextions correspond to (003) and (006) family planes, equivalent to the *d* spacing of full and half stacked brucite-like sheets [18].

Similar patterns were reported for analogous type structures [6,19]. However, the coprecipitation results in the formation of secondary phase identified as Cu hydroxyl carbonate, malachite structure (JCPDS#41-1390). It was reported, that the presence of Cu^{2+} excess could result in the formation of distorted octahedral structures due to the strong Jahn Teller effect shown by Cu^{2+} cations [20]. This results in structures like malachite where the triangular $(CO_3)^{2-}$ groups are surrounded by three sharing edges $Cu(OH)_6$ octahedra. The formation of this structure seems to indicate that the brucite layer was not able to accommodate all copper atoms. Costantino et al. [21] observed similar effect and deduced that brucite layer cannot tolerate the presence of two contiguous distorted $Cu(OH)_6$ octahedra and that the synthesis of Cu-rich hydrotalcites results either in low crystalline hydrotalcite or in Cu segregation in other copper containing phases. With the increase of the M^{2+}/M^{3+} ratio from HTCu1 to HTCu3 and consequent Al decrease, the proportion of malachite phase seems to increase for a constant hydrotalcite proportion, indicating the incorporation of all extra Cu^{2+} into hydroxyl carbonate like structure. No matter the nature of the obtained Cu, Zn and Al crystalline phases, the metals could be considered atomically dispersed in the continuous phase. When these phases are calcined at 350 °C the formation of CuO and ZnO phases of smaller size dispersed on alumina matrix is expected (Fig. 1B).

After calcination, the crystalline domains of hydrotalcite and malachite are no longer observed and the obtained diffractions are ascribed to copper species mainly CuO (JCPDS #48-1548) and $CuAl_2O_4$ (JCPDS #01-1153). The absence of any crystalline zinc or aluminium oxide phases indicates that both are incorporated as amorphous Zn-Al mixed oxides. The latter, is confirmed by the increase of the apparent crystallinity with the increase of M^{2+}/M^{3+} ratio for a constant Cu^{2+}/Zn^{2+} ratio, in a way that the lower the ratio the higher the amorphous component observed in diffraction pattern. The predominant presence of CuO detected for the HTCu3 sample also supports this statement. However, the presence of low crystalline phase containing Zn an Al, cannot be ruled out entirely, as the shape of the patterns suggests its contribution to the intense CuO diffraction. For a similar systems Melián-Cabrera et al. [22], suggested la formation of ZnO disordered phase produced after possible incorporation of small amount of Cu^{2+}.

Upon gold deposition (Fig. 1C), the diffraction pattern of all the samples resembles that of bulk CuO without any visible contribution of crystalline phase attributed to gold metal (ca. 38, 45 and 65° 2Θ). The latter indicates small particle size typically beyond the resolution limit of the diffractometer (< 4 nm).

Overall, it seems that after two calcination steps (one for the supports and one for the gold based catalysts) the samples are composed of small gold particles dispersed on mixed Cu-Zn-Al oxide matrix with well-defined CuO domains.

3.3. Transmission electron microscopy

The performed TEM analysis shows homogenous distribution of gold particles over mixed oxide support with an average gold particle size of 3.5 ± 0.3 nm for all the samples. The representative images and gold particles size distribution are presented in Fig. 2. The latter corroborates the XRD discussion. Indeed, gold deposition and the multiple calcination steps do not influence the catalyst structure, the samples are composed of small gold particles dispersed on well-defined CuO nanodomains (22–25 nm) embedded in ZnO-Al_2O_3 matrix. The performed mapping and EDS analysis of one selected sample (Supporting info Table S1 and Fig. S1) confirms the homogeneous metal dispersion and uniform gold particle size.

3.4. Redox properties: H_2-TPR

Water gas shift is complex redox process that requires catalysts with oxygen mobility and enhanced redox properties. In this sense, H_2-TPR experiments of the studied samples were carried out to evaluate the catalysts' reducibility and the interaction among the active species (Fig. 3). For the mixed oxides samples a single reduction profile was detected and typically attributed to the CuO → Cu reduction [23]. For the HTCu1 and HTCu2 samples this reduction process is centered ca. 250 °C while the HTCu3 sample seems to undergo a retarded reduction leading to a broad process between 270 and 420 °C. The latter is likely due to the slow hydrogen diffusion through the Cu°/CuO border due to the higher Cu loading in this material. Interestingly, the HTCu2 reduction profile is narrower indicating a more homogenous reducibility for this sample. Redox properties are remarkably boosted when gold is

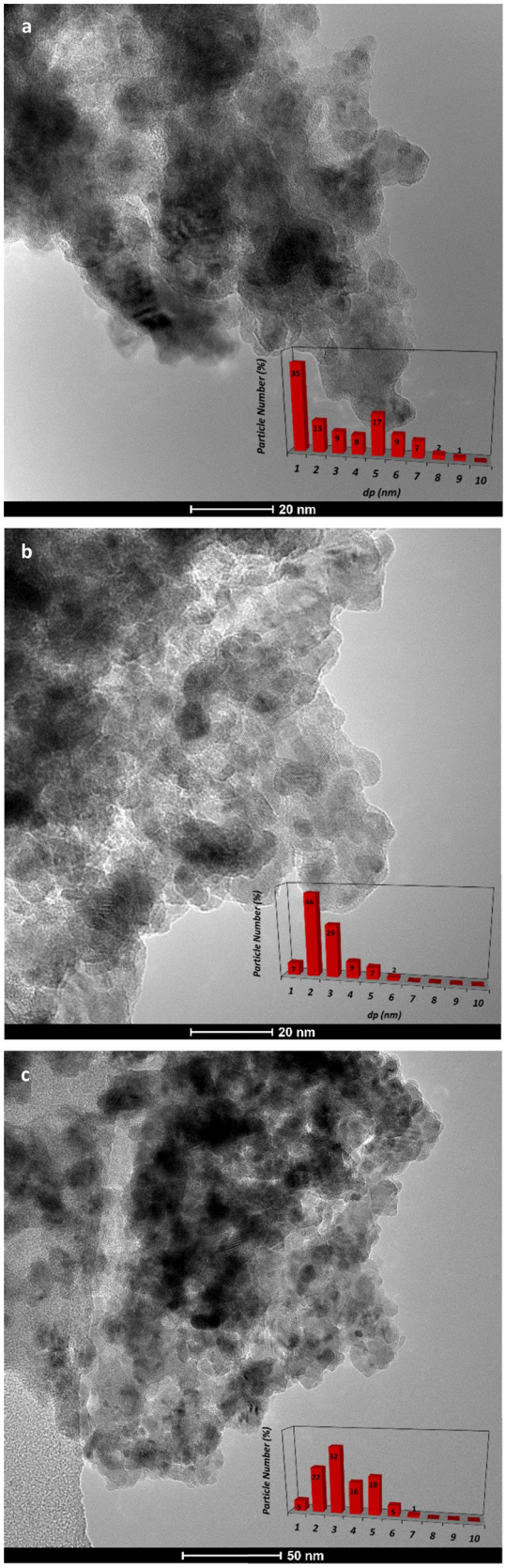

Fig. 2. TEM Micrographics **a.** AuHTCu1, **b**. AuHTCu2 and **c.** AuHTCu3.

added to the formulation. Indeed, all the reduction processes are shifted towards lower temperatures typically around 190 °C. In fact, the presence of gold is often reported to facilitate the H species mobility and also to weaken the Cu−O bond due to the electronic transfer between the oxide and the noble metal resulting in an overall improved reducibility [6,24,25]. Gold also helps HTCu3 to get closer to the behavior exhibited by HTCu1 and HTCu2.

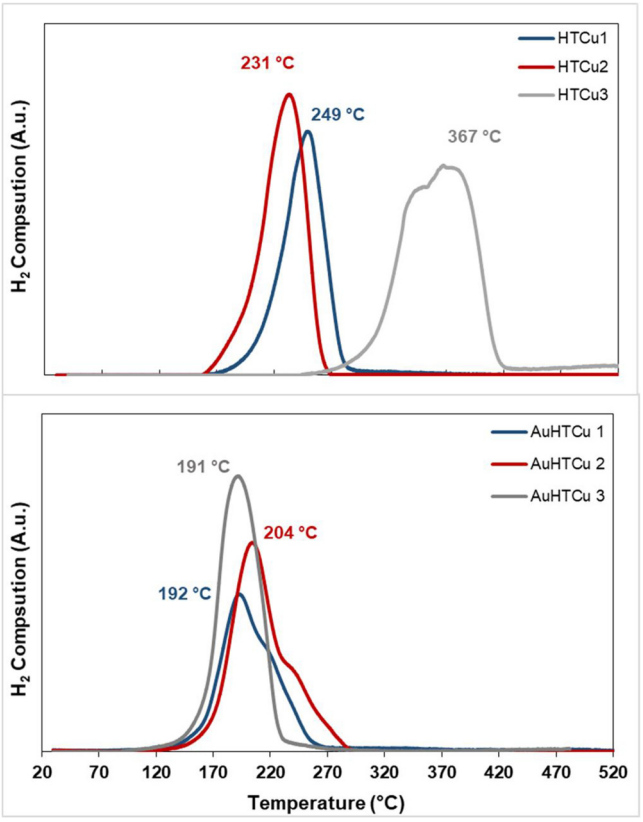

Fig. 3. TPR of the studied samples.

3.5. X ray photoelectron spectroscopy (XPS)

The electronic state of the catalyst surface of two representative samples HT2 and HT3 and their Au containing analogues are investigated by XPS at room temperature and after reduction at 150, 250 and 350 °C (Fig. 4). Our particular interest is focused on the Cu and Au state and their possible interaction during pretreatment. For the HTCu2 sample in the zone of Cu 2p, the Cu $2p_{3/2}$ y Cu $2p_{1/2}$ contributions (9339 and 9538 eV) accompanied by their satellites are observed on both, room temperature and reduced at 150 °C. First of all, the satellite presence unequivocally indicates the presence of cationic Cu^{2+} species but the shift of the Cu $2p_{3/2}$ at 150 °C to 9329 eV indicates an intermediate Cu state more reduced than Cu^{2+} but still not Cu° (with binding energy of 9319) [26]. Due to the similarity of the XPS spectra of Cu^{+} and Cu° it is complicated to affirm the prevalence of one or another but with the help of Auger spectra we could confirm at least their presence. The Auger spectra are presented in the supporting information (Fig. S2). If we consider the last obtained spectra (after reduction at 350 °C) is only due to metallic copper state the differences observed in the Auger spectra at lower temperatures are due to the presence of Cu^{2+} and Cu^{+}. One can discern that at 150 °C only the cationic states of copper coexists (Cu^{2+} and Cu^{+}) being the contribution at around 916 eV attributed to Cu^{+} species. Those oxidized species are reduced to Cu° at 250 and 350 °C, confirmed by satellites disappearing and Cu 2p signals shifting to lower binding energy (9319 eV for Cu $2p_{3/2}$).

For the HTCu3 sample all these features at 150 °C were not observed and the presence of the Cu^{+} is not confirmed suggesting that during reduction only Cu^{2+} and Cu° coexists. If we compare the intensity of the

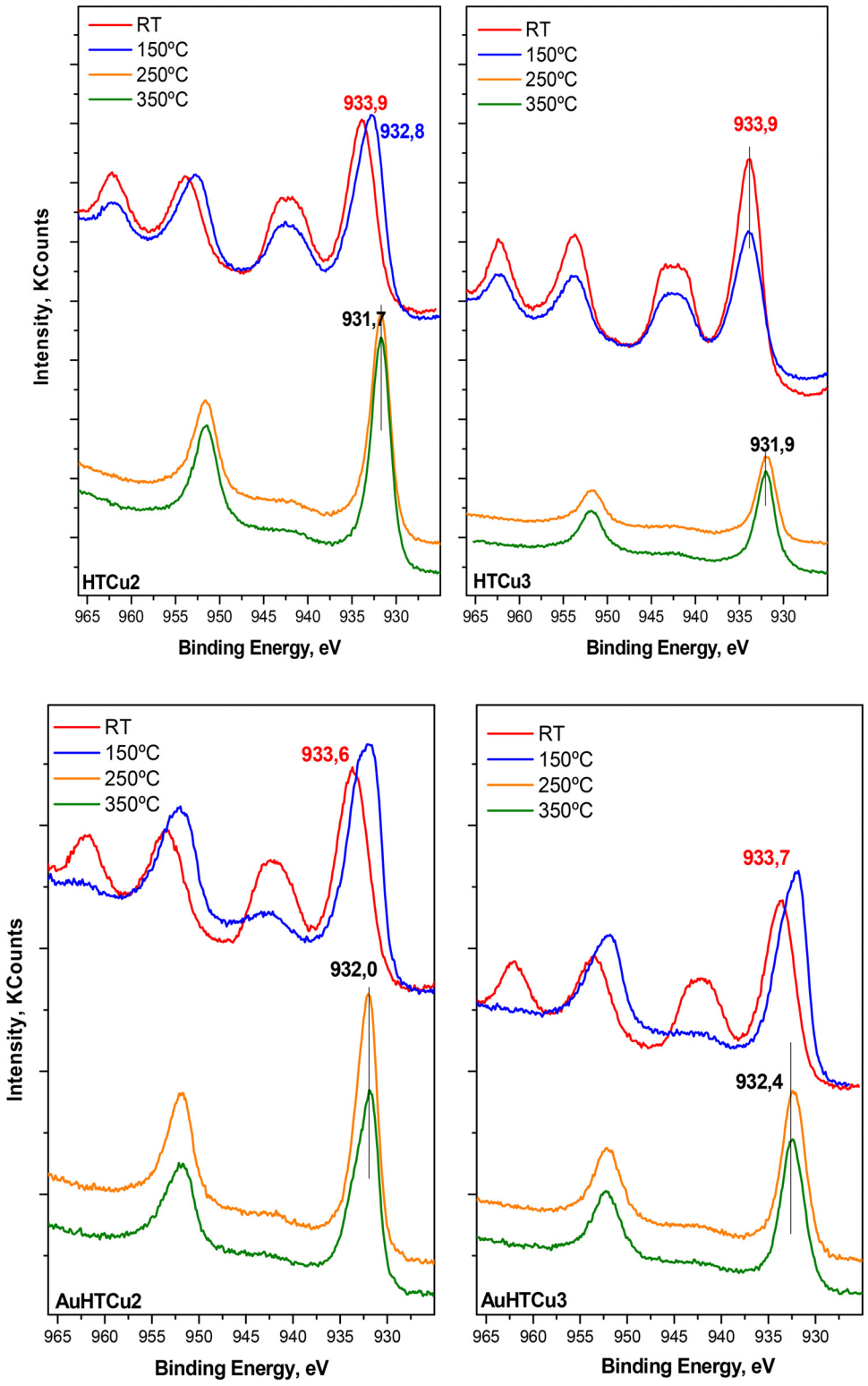

Fig. 4. XPS spectra of Cu 2p for HTCu2,HTCu3 and AuHTCu2 and AuHTCu3 samples.

signals (same scale for both samples), the lower signal for the HTCu3 at higher temperature indicates that this samples present less copper on the surface for a higher initial content suggesting an important sintering during the pretreatment.

However when gold is present the reduction of both samples is much more accelerated (as observed by TPR) and the copper states at 150 °C are predominantly Cu° with some small fractions of Cu^{2+} (also confirmed by the Auger spectra). As for gold at room temperature (illustrated by Au $4d_{5/2}$ and Au $4d_{3/2}$ in Fig. S4 in supporting information) the contribution unequivocally suggest the presence of metallic gold (Au $4d_{5/2}$ 335.5). With the temperature (Fig. S3 in supporting information) gold remains metallic although a shift to lower binding energy is observed suggesting cationic gold. This suggestion in H_2 presence results improbable but could be explained by a possible electron transfer from Au to Cu.

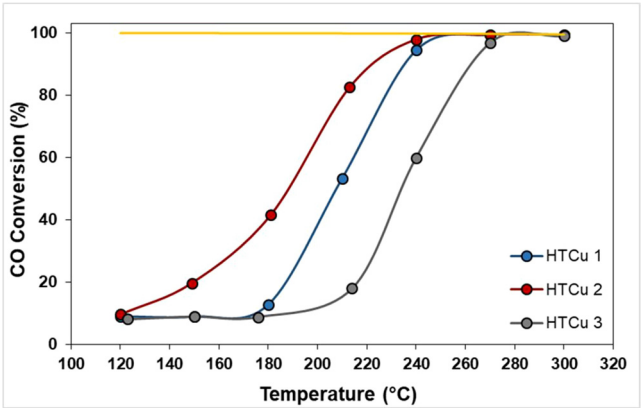

Fig. 5. WGS behavior of the prepared HT based catalysts in model WGS conditions (4,5% CO, 30% H_2O, and N_2 as balance GHSV 4000 h^{-1}).

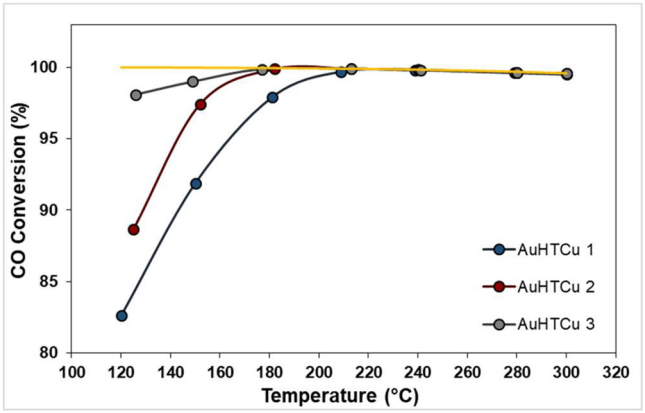

Fig. 6. WGS behavior of the prepared gold based catalysts in model WGS conditions 4,5% CO, 30% H_2O, and N_2 as balance GHSV 4000 h^{-1}).

3.6. Catalytic activity

One of the main drawbacks of CuO-ZnO benchmark catalysts in the water gas shift reaction is the need of pre-activation treatment. Nevertheless, if hydrogen is produced during the initial stages and sufficient temperature is applied (i.e. over 200 °C) the catalyst could achieve quickly its active state. In view of our TPR profiles Cu reduction is expected and the catalysts can be "in-situ" conditioned. However, in these conditions the observed CO conversion can be due also to parallel effects as for example CuO reduction ($CuO + CO \rightarrow CO_2 + Cu$). Considering the latter, the catalysts were tested in two consecutive runs to ensure that the Cu reduction do not interfere the results and the 2nd run is always presented. Under these premises, the WGS test was performed without activation steps reaching good levels of conversions as pictured in Fig. 5.

As anticipated by the TPR results, the redox properties matches rather well the exhibited WGS performance being the catalyst with higher oxygen mobility (i.e HTCu2) the best system within the studied series. Indeed, HTCu1 and HTCu2 reached equilibrium conversion at relatively low temperature ca. 240 °C. On the contrary the HTCu3 presents a broader operational window requiring higher temperatures (around 260 °C) to display equilibrium conversion. This is probably due to the hampered reduction of CuO in this sample as compared to the others.

The improved redox properties introduced by gold addition plus the inherent gold activity in the shift process greatly influence the catalytic trend (Fig. 5).

The activity curves dramatically shift towards low temperatures reaching equilibrium conversions at temperatures as low as 170 °C – an excellent result for low temperature shift converter. The exhibited activity trend AuHTCu3 > AuHTCu2 > AuHTCu1 correlates directly with the Cu loading as all the copper is reduced and available for reaction as confirmed by TPR and XPS. However, in view of the results the best trade-off is achieved with the AuHTCu2 material which present comparable activity for lower copper content (Fig. 6).

For realistic application, a post reforming mixture including H_2 and CO_2 must be considered. Fig. 7 represents the catalytic activity of our gold promoted catalysts in surrogate reforming mixture.

Similarly, to the results obtained for the model mixture, the catalytic trend evidences the superiority of the AuHTCu2 material. This sample achieves equilibrium conversion at 150 °C a great achievement for a shift catalyst that would permit an overall energy efficiency improvement of the fuel processor. On the contrary, the catalyst with highest Cu loading suffers deactivation in the high temperature range likely due to Cu particles sintering and loss of apparent activity. Such an effect starts at 220 °C when the catalyst is supposed to be fully reduced according to the TPR. As for AuHTCu1, it represents an intermediate

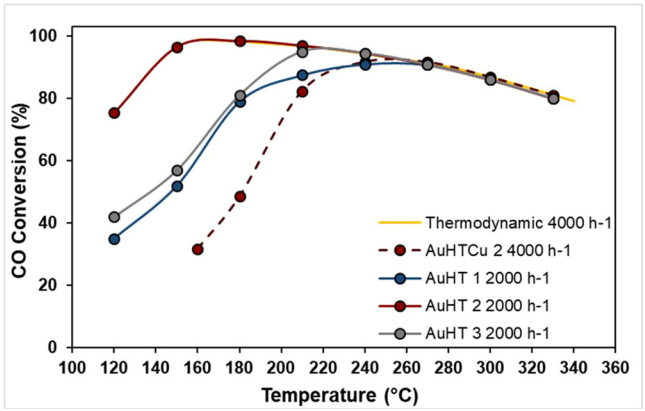

Fig. 7. WGS behavior of the prepared gold based catalysts at in simulated post-reforming mixtures (9% CO, 30% H_2O, 11% CO_2 and 50% H_2 GHSV 2000 h^{-1} and 4000 h^{-1} dashed line).

behavior displaying full CO conversion levels at 230 °C, still an acceptable temperature for a low temperature WGS system.

The promising results exhibited by the AuHTCu2 suggests a possible process intensification via increased space velocity which in turns would shrink the reactor volume making the fuel processor lighter and therefore suitable for portable applications. As shown in Fig. 7 (dashed lines) doubling the space velocity shifts the operation window to 230 °C which is still within the acceptable temperature scale for this process.

3.7. Long term stability test

One of the main characteristics that a catalyst must present to be implemented in portable fuel processor is to be stable for long term operations. Therefore, according to the obtained catalytic activity data, the most promising catalyst (AuHTCu2) was selected and tested to a long stability test under "realistic" conditions at 200 °C, during 45 h at GHSV of 4000 h^{-1} (Fig. 7).

As show in the plot, the activity weakly drops during the time required to achieve a steady state (the first 20 h of operation) [6]. Later on, the CO conversion becomes reasonably stable keeping high conversion (ca. 70% CO) during 45 h of reaction. Apparently, the AuHTCu2 catalysts does not get deactivated once reaching the steady state, preserving high conversion during the next 25 h under realistic post-reforming WGS mixture.

3.8. Start/stop cycles test

Nowadays, the start/stop stability test constitutes the most

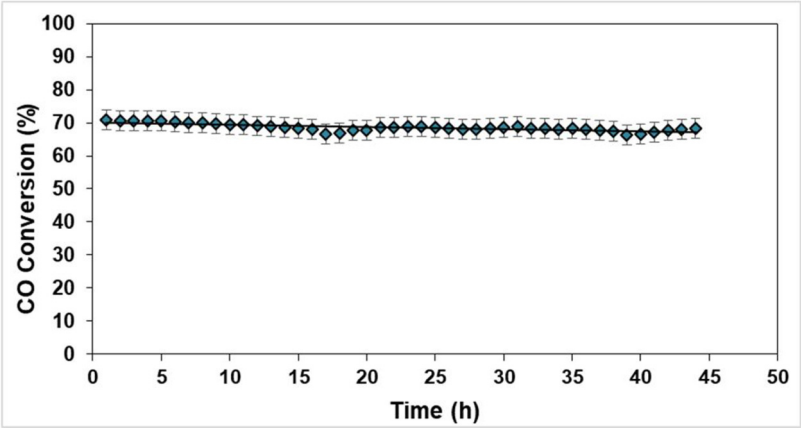

Fig. 8. Long term stability test of the most active sample at 230 °C (9% CO, 30% H_2O, 11% CO_2 and 50% H_2 GHSV 4000 h^{-1}).

aggressive test that can be imagined for a shift catalyst since during the stop stages the reactor is cooled down at room temperature with the reactive mixture flowing through the catalytic bed. Despite this kind of tests seems essential for practical reasons and they often represent a bottle neck for real applicability, they are not yet extended enough and only few reports can be found in literature [2,6,27,28]. To test the AuHTCu2 catalyst activity and stability 5 cycles of cooling down/heating up are carried out consecutively, being the 0 cycle the fresh state of the catalyst. During the cooling down the reactor was kept at room temperature for 30 min to ensure the condensation of water in catalytic bed. The results, in Fig. 8, show that AuHTCu2 catalyst successfully withstands the start/stop operations with no evidence of activity depletion after 5 cycles, remaining stable at around 70% CO conversion. We can then conclude that the AuHTCu2 is a promising robust catalyst that reasonably stands start-up/shut-down operations.

In summary, it seems that this catalyst is a very effective system for the low-temperature WGS process. The AuHTCu2 formulation results in the optimal active components composition exhibiting remarkable activity and stability for continuous applications and very importantly guarantees tolerance to transient start-up/shut down situations. Several reasons may account for the catalyst' overall good performance: (i) the suitability of the Cu-Zn-Al hydrotalcite like precursor for the generation of homogeneously distributed mixed oxides with optimal microstructure and metallic dispersion as confirmed by the TEM analysis and mapping, (ii) the cooperative effect established between gold and mixed oxides; in such a way that gold enhances Cu reducibility, leading to the formation of the active phase at lower temperature and suppressing the need of pre-activation since Cu is reduced in-situ under the reaction flow as confirmed by the XPS and H_2-TPR analysis (iii) the optimized $M^{2+}/M3^{+}$ ratio of 2 where the lower copper content is compensated by the gold presence and the existence of important Au/Cu active interphase, where a possible electron transfer is suggested by the XPS analysis; (iv) the recognized efficiency of nanogold for the oxidation reactions and (v) the co-existence of two active phases, gold and copper providing two routes for CO elimination (Fig. 9).

In fact, the strong Au-Cu contact may result in charge transfers between both metals creating a separation of the charges on the interface suitable site for reactants adsorption and activation [29]. The key point seems to be not only the gold assistance for rapid metallic copper formation but also the fact that gold supported on partially reduced copper (CuOx) is an excellent catalyst for the water gas shift [17].

4. Conclusions

The main goal of the study is successfully achieved - an optimal gold/copper based catalytic system is prepared. The use of hydrotalcite type precursor allows homogeneous catalysts' microstructure and enhanced metal-oxide contact. The noble metal addition facilitates CuO reduction at the early stages of reaction and ensures the presence of two active phases (Cu and Au) avoiding the requirement for catalyst conditioning before reaction. All prepared systems show excellent shift activity at low temperatures being the M^{2+}/M^{3+} ratio of 2 the optimal balance. In addition to the high CO conversion, the system is stable in both, long term and star-up/shut-down situations - a crucial prerequisite for a real application in fuel processor. Overall, the combination of Au and commercial-like Cu-Zn-Al formulation prepared from hydrotalcite precursor leads to a new generation of WGS catalysts with potential impact in the development of hydrogen technology.

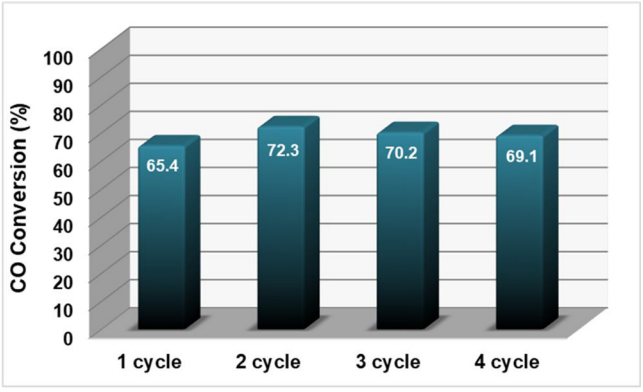

Fig. 9. Start/Stop cycles for AuHTCu2 catalyst (9% CO, 30% H_2O, 11% CO_2 and 50% H_2 GHSV 4000 h^{-1}).

Acknowledgements

Financial support for this work has been obtained from the Spanish Ministerio de Educación y Competitividad (MEC) (ENE2012-374301-C03-01) and (ENE2013-47880-C3-2-R) co-financed by FEDER funds from the European Union. The authors affiliated at Institute of Catalysis gratefully acknowledge financial support by theBulgarian Science Fund (Project ДН 09/5). T.R. Reina acknowledges the financial support from EPSRC through the grant EP/R512904/1.

Appendix A. Supplementary data

Supplementary material related to this article can be found, in the online version, at doi:https://doi.org/10.1016/j.apcata.2018.04.002.

References

[1] G. Kolb (Ed.), Fuel Processing for Fuel Cells, 434 Wiley-VCH, Weinheim, 2008.
[2] R. Farrauto, S. Hwang, L. Shore, W. Ruettinger, J. Lampert, T. Giroux, Y. Liu, O. Ilinich, Annu. Rev. Mater. Res. 33 (2003) 1–27.
[3] V. Mehta, J.S. Copper, J. Power Sources 114 (2003) 32–53.
[4] L. Wang, K. Murata, M. Inaba, J. Power Sources 145 (2005) 707–711.
[5] D.K. Liguras, D.I. Kondarides, Xenophon E. Verykios, Appl. Catal. B. 43 (2003) 345–354.
[6] J.L. Santos, T.R. Reina, S. Ivanova, M.A. Centeno, J.A. Odriozola, Appl. Catal. B Environ. 201 (2017) 310–317.
[7] K.M. VandenBussche, G.F. Froment, J. Catal. 161 (1996) 1–10.
[8] C. Wang, C. Liu, W. Fu, Z. Bao, J. Zhan, W. Ding, K. Chou, Q. Li, Catal. Today 263 (2015) 46–51.
[9] C. Ratnasamy, J. Wagner, Catal. Rev. Sci. Eng. 51 (2009) 325–440.
[10] D.L. Trimm, Appl. Catal. A 296 (2005) 1–11.
[11] T.R. Reina, S. Ivanova, J.J. Delgado, I. Ivanov, V. Idakiev, T. Tabakova, M.A. Centeno, J.A. Odriozola, ChemCatChem 6 (2014) 1401–1409.
[12] R.J. Farrauto, Y. Liu, W. Ruettinger, Catal. Rev. Sci. Eng. 49 (2007) 141–196.
[13] A.R. Martins, L.S. Carvalho, P. Reyes, J.M. Grau, M.C. Rangel, J. Mol. Catal. A Chem. 429 (2017) 1–9.
[14] R. Burch, Phys. Chem. Chem. Phys. 8 (2006) 5483–5500.
[15] J. He, M. Wei, B. Li, Y. Khang, D.G. Evans, X. Duan, Struct. Bond. 119 (2006) 89–119.
[16] M. Behrens, L. Kasatkin, S. Kuhl, G. Weinberg, Catal. Chem. Mater. 22 (2010) 386–397.
[17] D. Andreeva, V. Idakiev, T. Tabakova, L. Ilieva, P. Falaras, A. Bourlinos, A. Travlos, Catal. Today 72 (2002) 51–55.
[18] A. Tsyganok, A. Sayari, J. Solid State Chem. 179 (2006) 1830–1841.
[19] A. Vaccari, Appl. Clay Sci. 14 (1999) 161.
[20] U. Costantino, F. Marmottini, M. Sisani, T. Montanari, G. Ramis, G. Busca, M. Turco, G. Bagnasco, Solid State Ionics 176 (2005) 2917–2922.
[21] I. Melián-Cabrera, M. López Granados, J.L.G. Fierro, Phys. Chem. Chem. Phys. 4 (2002) 3122–3127.
[22] A.L. Boyce, S.R. Graville, P.A. Sermon, M.S.W. Vong, React. Kin. Catal. Lett. 44 (1991) 1–11.
[23] Q. Fu, S. Kudriavtseva, H. Saltsburg, M. Flytzani-Stephanopoulos, Chem. Eng. J. 93 (2003) 41–53.
[24] D. Andreeva, I. Ivanov, L. Ilieva, J.W. Sobczak, G. Avdeev, T. Tabakova, Appl. Catal. A 333 (2007) 153–160.
[25] T. Giroux, S. Hwang, Y. Liu, W. Ruettinger, L. Shore, Appl. Catal. B 55 (2005) 185–200.
[26] NIST X-ray Photoelectron Spectroscopy Database, Version 4.1 (National Institute of Standards and Technology, (2012) Gaithersburg http://srdata.nist.gov/xps/.
[27] S. Collussi, L. Katta, F. Amoroso, R.J. Farrauto, A. Trovarelli, Catal. Comm. 47 (2014) 63–66.
[28] Y. Li, Q. Fu, M. Flytzani-Stephanopoulos, Appl. Catal. B 27 (2000) 179–191.
[29] T. Reina, S. Ivanova, M.A. Centeno, J.A. Odriozola, Appl. Catal. B Environ. 187 (2016) 98–107.